Heat transfer from nanoparticles: A corresponding state analysis

Samy Merabia[a], Sergei Shenogin[b], Laurent Joly[a], Pawel Keblinski[b], and Jean-Louis Barrat[a,1]

[a]Laboratoire de Physique de la Matière Condensée et des Nanostructures, Centre Nationale de la Recherche Scientifique, Unité Mixte de Recherche 5586, Université de Lyon, 43 Boulevard du 11 Novembre 1918, 69622 Villeurbanne Cedex, France; and [b]Rensselaer Nanotechnology Center and Department of Materials Science and Engineering, Rensselaer Polytechnic Institute, Troy, NY 12180

Edited by Stuart A. Rice, University of Chicago, Chicago, IL, and approved May 29, 2009 (received for review February 6, 2009)

In this contribution, we study situations in which nanoparticles in a fluid are strongly heated, generating high heat fluxes. This situation is relevant to experiments in which a fluid is locally heated by using selective absorption of radiation by solid particles. We first study this situation for different types of molecular interactions, using models for gold particles suspended in octane and in water. As already reported in experiments, very high heat fluxes and temperature elevations (leading eventually to particle destruction) can be observed in such situations. We show that a very simple modeling based on Lennard–Jones (LJ) interactions captures the essential features of such experiments and that the results for various liquids can be mapped onto the LJ case, provided a physically justified (corresponding state) choice of parameters is made. Physically, the possibility of sustaining very high heat fluxes is related to the strong curvature of the interface that inhibits the formation of an insulating vapor film.

interfaces | liquids | Kapitsa resistance

Submicron-scale heat transfer is attracting a growing interest, motivated by both fundamental and technological points of view. In fluids, considerable attention has been devoted to the so-called nanofluids (1, 2), in which nanoparticles in dilute suspension appear to modify both bulk heat transfer and critical heat fluxes. Although the former effect can presumably be understood in terms of particle aggregation (3, 4), the latter is still poorly understood.

More generally, heat transfer from nanoparticles or nanostructures to a fluid environment is a subject of active research, stimulated by the development of experimental techniques such as time-resolved optical absorption or reflectivity or photothermal correlation spectroscopy (5). Applications include, e.g., the enhancement of cooling from structured surfaces, local heating of fluids by selective absorption from nanoparticles, with possible biomedical hyperthermia uses (6, 7). Recent experiments demonstrated the possibility of reaching very high local temperatures by using laser heating of nanoparticles (8–10), even reaching the melting point of gold particles suspended in water. From a conceptual point of view, such experiments raise many interesting questions compared with usual, macroscopic heat-transfer experiments. How are the phase diagram and heat-transfer equations modified at small scales? How relevant is the presence of interfacial resistances, and how do they change with temperature?

The case of nanofluids (11) is a good illustration of the role that can be played by molecular simulation in the interpretation of such complex situations. Although many interpretations have been proposed to explain the reported experimental results, it is only simulation of simple models that has been able to disprove some of these interpretations and to demonstrate the validity of the alternative, aggregation scenario. Interestingly, the use of complex models with accurate interaction force fields is not, in general, needed to answer the basic qualitative questions raised by such experimental approaches.

In this article, we use molecular simulation to study the heat transfer from solid nanoparticles to a surrounding fluid under extreme conditions (high heat fluxes) using both realistic and simplified molecular models. We show that, in agreement with experiments, the temperature of nanometer-sized particles can be elevated considerably without inducing bubble nucleation in the fluid. This feature is contrasted with the situation for flat surfaces, at which an instability leading to the formation of an insulating vapor layer takes place at much smaller heat fluxes and temperatures (12, 13). Using a comparison between a "realistic" description of gold–octane and gold–water systems and of a simplified Lennard–Jones (LJ) model, we show, based on a "corresponding state" analysis, that the features observed are quite universal. A simple mapping using critical temperature, interfacial, and heat conductivity properties of the particle/solvent pair allows one to reproduce accurately the behavior of different systems.

Gold Nanoparticles in Octane

To establish a connection with experimental reality, we began by using molecular dynamics to simulate heat transfer from a model gold nanoparticle into octane solvent. The selection of a relatively simple organic solvent in this first part, rather than water, is motivated by the fact that molecular models are quite accurate in predicting liquid–vapor phase diagrams for alkanes. Our model consists of a nanoparticle, with an average radius of $\approx$1.3 nm, containing 494 gold atoms arranged on a face centered cubic (FCC) lattice with density 19.5 g/cm^3. The nanoparticle is immersed in liquid octane containing 2,721 octane molecules (21,768 united carbon–hydrogen atoms) and placed in a cubic simulation cell with periodic boundary conditions. The interactions between united atoms forming octane molecules are described by the Amber force field (14) with all nonbonded interaction energy calculated according to 6–12 LJ. The interaction between gold atoms was also described by a 6–12 LJ potential, fitted to reproduce bulk Au density (19.5 g/cm^3) and the melting point (1,310 K). Finally, the interaction potential between octane-united atoms and gold atoms was adapted from ref. 15. All simulations were carried out at constant pressure of 1 atm and with the integration time step of 2 fs. In the equilibration stage of the simulation, a global thermostat is used to maintain the overall temperature at 300 K. The equilibration stage takes $\approx$1 ns, and under 1 atm, the equilibrated system is contained in a cubic simulation box with the edge length of $\approx$90 Å. The nanoparticle is initially placed in the center of the simulation cell but is allowed to freely diffuse during the simulations. The equilibrium density of the model octane fluid is equal to 0.71 g cm^{-3}, which compares well with the experi-

Author contributions: P.K. and J.-L.B. designed research; S.M., S.S., L.J., P.K., and J.-L.B. performed research; S.M., S.S., P.K., and J.-L.B. analyzed data; and S.M., P.K., and J.-L.B. wrote the paper.

The authors declare no conflict of interest.

This article is a PNAS Direct Submission.

[1]To whom correspondence should be addressed. E-mail: barrat@lpmcn.univ-lyon1.fr.

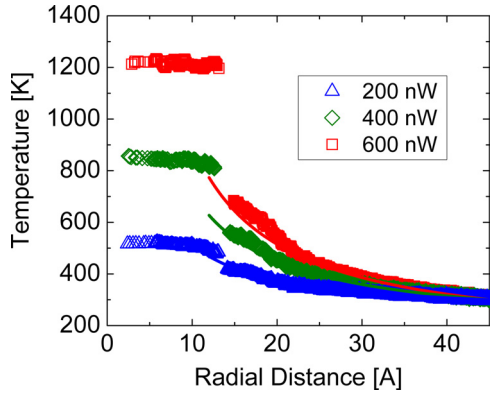

Fig. 1. Steady-state temperature profiles for octane–gold model system at 3 heating power levels (symbols) and fits with the continuum theory prediction $T(r) = A + B/r$ (solid lines).

mental density of 0.7025 g cm^{-3}. To study the heat flow from the nanoparticle to the solvent, the nanoparticle was heated, with a constant heating power in the range of 100-1000 nW, by rescaling of the atomic velocities every time step. The liquid octane in the periphery of the system, at distances >40 Å from the nanoparticle center (taking into account a possible diffusive motion), was maintained at 300 K, thus providing the heat sink. Up to heating powers of 700 nW, after a transient of ≈100 ps, a steady state is established. In the steady state, we collect time averages (over 1 ns) of density and temperature profiles obtained for spherical shells concentric with the nanoparticle center and with a thickness of 2 Å. For heating powers >700 nW, the system was unstable, and its behavior will be described below.

Steady-state temperature profiles for P = 200, 400, and 600 nW heating powers are presented in Fig. 1. The temperature profiles have several noteworthy features. First, the temperature of the nanoparticle is more or less uniform; this is an effect of the relatively high thermal conductivity of crystalline solid, as compared with liquid. We mention here that the electronic contribution to the conductivity, which provides the dominant mechanism of heat conduction within metallic nanoparticles, is not accounted for in our description. The essential point, however, is that the conductivity of the solid is much higher than that of the liquid, independent of the precise mechanism involved. Second, the temperature in the liquid follows the solution of the continuum heat flow problem with spherical symmetry (see solid lines in Fig. 1). In the steady state, the temperature profile is described by the solution of the Laplace equation in the form:

$$T(r) = A + B/r. \quad [1]$$

Near the particle–liquid interface, the temperature profile deviates from the formula given by the Eq. **1**, particularly for larger heating powers involved. This deviation is likely due to the nonuniform thermal transport properties of the liquid, because Eq. **1** is valid under the assumption that the thermal conductivity is constant. Very importantly, there is a large temperature drop, ΔT, at the nanoparticle–liquid interface, which is a manifestation of the interfacial thermal resistance. Such resistance is caused by the mismatch of thermal properties between the solid and liquid components and is also affected by the strength of the interfacial bonding. The interfacial thermal conductance, G, can be quantified via the relationship:

$$j_Q = G\Delta T, \quad [2]$$

where j_Q is the heat flux across the interface, and ΔT is the discontinuous temperature at the interface (see temperature

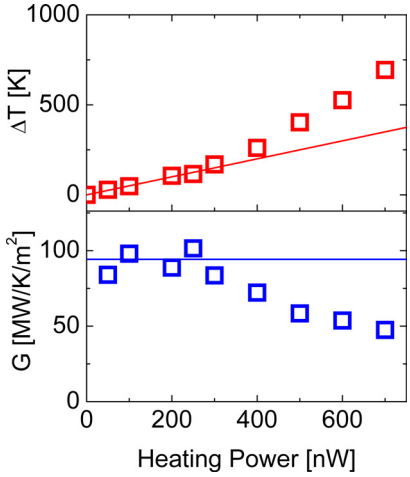

Fig. 2. Temperature drop at the interface for octane–gold model system (*Upper*) and calculated interface conductance (*Lower*) as a function of heating power. Lines represent linear response regime.

profiles in Fig. 1). Fig. 2 *Upper* shows the relationship between the heating power P and the temperature drop at the octane–liquid interface. At lower heating powers, the heat flux is proportional to the heating power, indicating constant value of the interfacial conductance. However, at >300-nW heating power, the increase in the temperature drop becomes steeper, indicating increasing interfacial thermal resistance (see Fig. 2).

The calculated interfacial conductance as a function of P is shown in Fig. 2 (*Lower*). At small heating powers (temperature drops), the value of the interfacial conductance is ≈100 MW/m^2/K. This value is similar to those obtained in an experiment on gold nanoparticle–water dispersions (16). With increasing heat power (temperature drop), the interfacial thermal conductance decreases from 100 to ≈50 MW/m^2/K at P = 700 nW. To gain an insight into the structural origin of the behavior, we show in Fig. 3 the octane density profiles corresponding to temperature profiles from Fig. 1. As the temperature of the nanoparticle and the adjacent liquid increases, there is a visible decrease of liquid density adjacent to the solid surface (see Fig. 3). This increase of the molecular distance between liquid molecules and solid atoms is likely responsible for the decrease of the interfacial thermal conductance.

Gold Nanoparticles in Water

To explore a different type of bonding for the liquid, to allow a connection to recent experiments (5), we explore in this section a system made of a gold nanoparticle similar to the one described in the previous section, solvated in water modeled using the

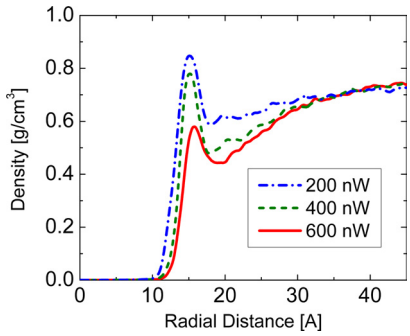

Fig. 3. Steady-state octane density profiles for octane–gold model system at 3 heating power levels.

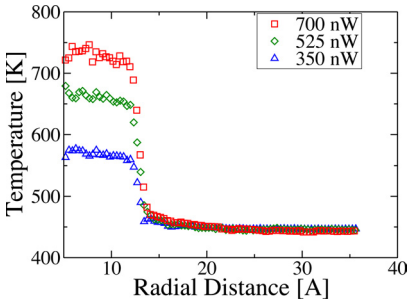

Fig. 4. Temperature profiles across the water–gold nanoparticle interface at 3 heating strengths.

standard SPC/E model (17). To allow comparisons with the LJ calculations described below, we studied water pressurized at a pressure of 80 bars and at a temperature of 450 K. These parameters were chosen so that the distance to the critical point is large but still within a range that allows comparisons between different models. The system was made of 10,000 water molecules.

The main issue here is the choice of the model for the gold–water interaction. Experimentally, the results reported for the wetting of water on gold are quite scattered, with, in general, a large contact angle hysteresis. Results obtained under UHV conditions (18, 19) report a low contact angle (<30° or close to a wetting situation). On the other hand, the force fields that exist in the literature, and have been based on density functional theory DFT calculations (12, 20), yield higher contact angles.

In this study, we make the choice of strengthening the attractive terms in these effective potentials to obtain a contact angle (estimated from a simple calculation of the LJ contributions to the surface tensions (21) and of a the actual value of the SPC/E surface tension at 300 K) of the order of 25°, consistent with experiments. As a result, the gold–water interaction is written in the form of a standard 6–12 potential like in ref. 20, with the following parameters: $\varepsilon_{O/Au} = 0.59$ kcal·mol^{-1} and $\sigma_{O/Au} = 0.36$ nm, whereas the hydrogen atoms do not interact with the gold atoms. The system NP plus water is first equilibrated during 100,000 time steps that represent a physical time of 200 ps. Then the nanoparticle is heated up at a constant power while the water molecules at a distance 20 Å from the nanoparticle are thermostated at 450 K. In all of the following, we will restrict ourselves to moderate heating powers (<700 nW), because for larger heating intensities, we have observed nonstationary effects in the heat transfer process. Although these effects are interesting in themselves, their study is beyond the scope of this article, and we leave a complete study for future work.

Temperature profiles of gold NP immersed in water, heated at various powers, are shown in Fig. 4. Clearly, temperature profiles are flatter in water than in octane, if the comparison is made at the same value of the heating power. This is due to the ≈5 times larger conductivity of water compared with octane. On the other hand, interfacial temperature jumps ΔT are smaller in the water/gold case. Note that it is essential to do the comparison at a given value of the heating power, not at a given value of the nanoparticle temperature. For instance, for the nanoparticle heated up at 400 nW in octane, we have measured $\Delta T = 220$ K, whereas it is a factor of 2 less if the nanoparticle is immersed in water. Consequently, the water/gold interface has a larger interfacial conductance than the octane/gold system. The value we have measured varies from $G = 170$ MW/m^2/K to $G = 150$ MW/m^2/K over the range of heating power investigated, a variation that is smaller than in the case of octane. This trend is consistent with the recent finding that the interfacial conductance increases with work of adhesion, which is higher for the gold–water case than for the gold–octane case (22). The Kapitsa length $l_K = \lambda/G$, where λ is the thermal conductivity, is of the order of 3.4 nm in this case and of 1 nm in the gold/octane case.

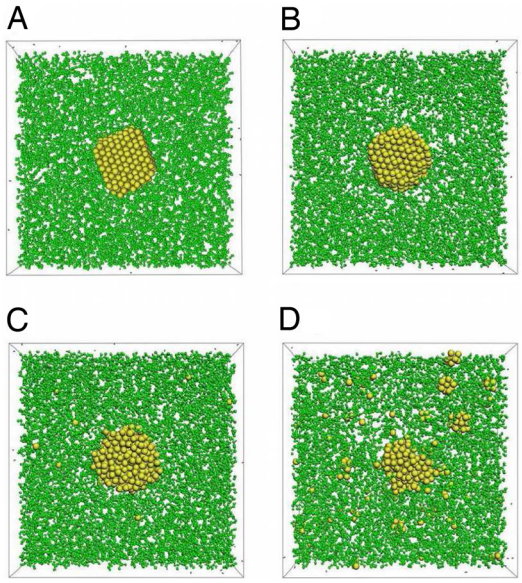

Fig. 5. Snapshots of octane–gold model system at heating powers of 0 nW (*A*), 500 nW (*B*), 700 nW (*C*), and 1000 nW (*D*).

Melting of the Nanoparticles

At high enough temperatures, experiments have illustrated the possibility of particle melting (9) within the fluid. We also explored briefly this issue in our simulations of gold particle in octane. By inspection, we observed that up to $P = 500$ nW, the nanoparticle structure remained crystalline. However, at $P = 600$ nW, the crystalline order of the nanoparticle is lost. At $P = 700$ nW, we observed that atoms from the nanoparticle surface are gradually "evaporated" into the solution. At a later stage, they recombine into small Au clusters (Fig. 5). We note that all these processes occur without formation of a liquid vapor interface, which, as discussed below, is caused by very large Laplace pressure. In fact, by using the surface tension of octane at room temperature $\gamma = 21.8 \times 10^{-3}$ N/m and a bubble radius of $R_0 = 2$ nm, one obtains the Laplace pressure of $P_L = 2\gamma/R_0 \simeq 200$ atm. This value is much larger than the critical octane pressure of 25.5 atm. These results illustrate an exciting possibility of decomposition of metal nanoparticles into metal atoms or small clusters, without explosive evaporation or thermal damage on the embedding medium. Interestingly, we have not observed such fragmentation for nanoparticles immersed in water. Although the crystalline order is lost, the gold nanoparticle keeps its integrity. This is probably due to the higher interfacial energy of the gold/water interface compared with gold/octane.

LJ Model

To emphasize the generality of the scenario described above, we briefly recall here the results obtained for a generic model of a simple, LJ monoatomic fluid in contact with a heated solid particle (13). The system is made of a FCC solid particle formed of 555 atoms, immersed in a fluid of 23,000 atoms, all of the atoms interacting through a LJ potential $V_{\alpha\beta}(r) = 4\,\varepsilon((\sigma/r)^{12} - c_\alpha\beta(\sigma/r)^6)$, where α, β refers to solid or liquid atoms. The potential has a cutoff radius 2.5 σ, where σ is the diameter of the atoms. The parameters ε and σ are taken to be the same for both phases. The parameter $c_\alpha\beta = 1$ if $\alpha = \beta$; $c_\alpha\beta = c_{FS}$ otherwise controls the wetting interaction between the fluid and the solid

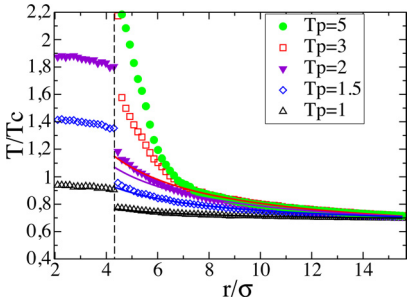

Fig. 6. Steady-state temperature field across the liquid/nanoparticle interface, obtained with the LJ model (adapted from the results of ref. 13). The temperature has been normalized by the critical temperature T_c of the LJ fluid. The position of the nanoparticle surface is indicated by dashed lines, r measuring the distance to the center of the nanoparticle. Solid curves correspond to fits by the continuum theory result $T(r) = A/r + B$. Note that for $T_p = 1$ and $T_p = 1.5$, the solid curves are almost indistinguishable from the simulation data. For the highest temperatures, the temperature field inside the particle is not shown in order to limit the amplitude of the scale of the vertical axis.

nanoparticle. In addition to the LJ interactions, atoms inside the particles are connected to their neighbors with FENE springs (23) $V(r) = -0.5kR_0^2 \ln(1 - (r/R_0)^2)$ with $k = 30\ \varepsilon/\sigma^2$ and $R_0 = 1.5\ \sigma$. This nearest-neighbor bonding allows one to heat up the nanoparticle to rather high temperatures without observing the melting or fragmentation phenomena mentioned above. In the following, we will concentrate on results obtained for $c_{FS} = 1$, which will be shown in *Corresponding States Analysis* to be an appropriate value for a mapping between the LJ and gold–octane systems. The dependence on c_{FS} is discussed in ref. 13. All results in this section are given in standard LJ units, ε/k_B, σ and $\tau = \sqrt{m\sigma^2/\varepsilon}$ for temperature, length, and time, respectively. Here, m is the mass of the fluid atoms.

We integrate the equations of motion using a velocity Verlet algorithm with a time step $dt = 0.005\tau$. All of the systems considered have been first equilibrated at a constant temperature $T_0 = 0.75$ under the constant pressure $P_0 = 0.015$ (using a Nose/Hoover temperature thermostat and pressure barostat). The temperature T_0 is below the boiling temperature, that we found to be $T_b \simeq 0.8$, using independent simulations of a liquid/vapor interface, under the pressure P_0 at which we are working. After 100,000 time steps of equilibration, the nanoparticle is heated up at different temperatures $T_p > T_b$ by rescaling the velocities of the solid particles at each time step while the whole system is kept at the constant pressure P_0 by using a NPH barostat. The fluid beyond a distance 10σ from the particle surface is thermostated at $T_0 = 0.75$, again by using velocity rescaling. Temperature, density, and pressure fields have been obtained by averaging the corresponding quantities during 10,000 time steps in nanoparticle centered spherical shells of width $\simeq 0.15\sigma$, after a steady state is reached. Finally, we calculate the heat flux density flowing through the solid particle, by measuring the power supply needed to keep the nanoparticle at the target temperature T_p.

Fig. 6 displays steady-state temperature profiles close to the nanoparticle surface, for different temperatures T_p of the nanoparticle. For low T_p, the temperature field in the liquid is practically indistinguishable from the form $A/r + B$ (Eq. **1**). The general behavior is strikingly similar to the one obtained for the gold–octane system. Inside the solid, the temperature is not uniform but slightly curved downwards because of the finite conductivity of the nanoparticle. As in the gold/octane simulation, the temperature is discontinuous at the interface. For a given value of the nanoparticle temperature T_p, the relative temperature jump ΔT is quite comparable with the gold–octane results, thus suggesting that the corresponding interfacial conductance is depends on the details of the nanoparticle/fluid interaction mostly trough macroscopic parameters such as the wettability (24–26). Similar indications can be found in ref. 22., where it was shown that the interfacial conductance of surfactant–water interfaces is directly proportional to the work of adhesion. For instance, for the nanoparticle heated up at $T_p = 1.5$, we have measured a temperature jump $\Delta T/T_c \simeq 0.4$ that is quite comparable with the value reported in Fig. 2 for the gold nanoparticle for the 400-nW heating power. Similarly, the value of the conductance obtained $G = j_Q/\Delta T \simeq 0.6$ is consistent with the gold/octane results displayed in Fig. 2, if we assume that a value of $G = 1$ in our LJ units corresponds to an interfacial conductance on the order of 100 MW/K/m^2. All these results suggest that the interfacial conductance is a quantity that does not strongly depend on the details of the nanoparticle/fluid interaction but only on generic properties of an interface as, e.g., the wettability. This correspondence between the simplified LJ system and the more realistic description of gold in octane will be explored further in the next section.

We also mention briefly that very high flux situations can be explored here thanks to the "covalent" bonding introduced between the atoms of the solid particle. Upon increasing the temperature of the nanoparticle, deviations from the $1/r$ behavior are clearly seen in Fig. 6, when the local temperature exceeds the critical temperature T_c. Interestingly, the temperature profile steepens close to the nanoparticle surface, corresponding to a decrease of the local effective conductivity. The density profile (13) differs somewhat from its octane or water counterparts, with density oscillations in the case of the monoatomic LJ fluid. These oscillations are smeared out for a molecular liquid. The most important point is that, even far above the critical point, we do not observe a steep decrease of the liquid density in the vicinity of the particle, but rather the appearance of a dilute liquid layer, with a density decreasing when the nanoparticle gets hotter. Note, however, that the density within this layer is still 1 order of magnitude larger than the vapor density at coexistence. Thus, even at temperatures several times T_c, boiling of the surrounding fluid is not observed.

Corresponding States Analysis

Obviously, the qualitative similarities between the observations in the previous sections points to a rather generic scenario. To allow a more quantitative comparison, a mapping between the different systems is necessary. The mapping we investigate will be based on the physical properties that dominate the problem under consideration, namely interfacial effects, liquid vapor coexistence, and heat transfer in the liquid phase.

We start by a discussion of the gold–octane case, which in view of the rather similar interactions, can be expected to be easily mapped onto a LJ system. The first step is to tune the interaction coefficient between fluid and solid, c_{FS}, to a value that is best suited to reproduce the properties of the gold–octane interface. Generally speaking, the wetting properties of an interface can be related to the interaction potential $u_{ij}(r)$ through the interfacial work (21) $H_{ij} = -(\rho_i\rho_j/4)\int_{r_0}^{+\infty} r u_{ij}(r) d\mathbf{r}$, where r_0 is a minimal radius of approach between 2 molecules, ρ_i and ρ_j denoting the number densities of the interacting media. The wetting properties (equilibrium contact angle or spreading parameter) will be determined by the ratio $r = H_{FS}/H_{FF}$. In the gold octane system, this ratio is

$$\frac{\rho_{Au}}{\rho_{CH_2}} \frac{\varepsilon_{CH_2/Au}}{\varepsilon_{CH_2/CH_2}} \frac{\sigma^6_{CH_2/Au}}{\sigma^6_{CH_2/CH_2}}.$$

In the latter expression, $\rho_{Au} = 0.1$ mol·cm^{-3} and $\rho_{CH_2} = 0.05$ mol·cm^{-3} are the gold and fluid number densities, $\varepsilon_{CH_2}/Au = 0.429$ kcal·mol^{-1}; $\varepsilon_{CH_2}/CH_2 = 0.143$ kcal·mol^{-1} are the octane

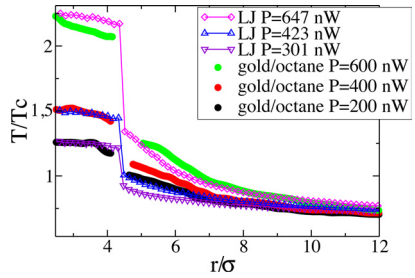

Fig. 7. Reduced temperature profiles across the gold/octane interface (filled symbols) compared with the profiles obtained with the LJ model (open symbols). T_c is the critical temperature of octane and of the LJ fluid respectively. For the gold/octane system, $\sigma = 0.32$ nm as discussed in the text. Here, the gold/octane system was thermostated at $T = 380$ K.

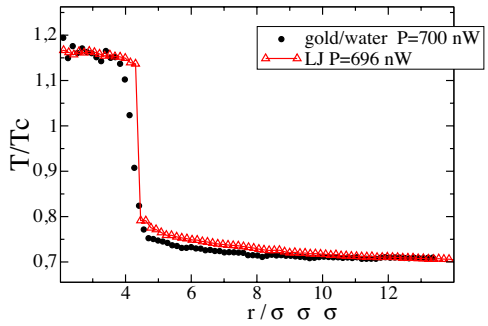

Fig. 8. Reduced temperature profiles across the gold/water interface (filled symbols) compared with the profiles obtained with the LJ model (open symbols). Here, $T_c = 650$ K and $\sigma = 0.22$ nm for water.

united atoms/gold and octane/fluid interaction energies (15), whereas $\sigma_{CH_2}/Au = 0.328$ nm; $\sigma_{CH_2}/CH_2 = 0.3923$ nm are the radii of the corresponding interaction. Hence, we find $r \simeq 2$. For the monoatomic LJ model, $r = c_{FS}\rho_S/\rho_F$, where the nanoparticle and liquid densities are, respectively, $\rho_S \simeq 1.46\sigma^{-3}$ and $\rho_L \simeq 0.76\sigma^{-3}$. To match the value of r, a value of parameter $c_{FS} \simeq 1$, as used in section 2, is therefore appropriate.

Now, we discuss the value of the unit of thermal flux used in the generic LJ model. To this end, we shall first determine the units of length, time, and energy σ, τ, and T corresponding to the generic model. Throughout, we denote by stars quantities expressed in LJ units where the units of length σ, time τ and energy ε are all set equal to 1. Alternatively, we can determine the values of σ, τ and ε by matching the thermal properties of the generic LJ model to the ones of the gold/octane model. By matching the critical temperature of the LJ model, $T_c^\star = 1.08$ to the octane critical temperature $T_c = 569$ K, we obtain the unit of energy, $\varepsilon/k_B = 527$ K. The values of the units of length and time are obtained by matching the values of the thermal conductivity λ and thermal diffusivity D_{th} of octane $\sigma^3 = D_{th}k_B/\lambda\ \lambda^\star\sigma^{\star 3}/D_{th}^\star k_B^\star$ and $\tau = k_B/\lambda\sigma\ \lambda^\star\sigma^\star\tau^\star/k_B^\star$. The thermal conductivity of the monoatomic LJ fluid $\lambda^\star = 0.36$ was measured by using stationary heat transfer simulations, whereas we have used the value $D_{th}^\star = 1$ for the thermal diffusivity reported in ref. 27. Using the values of the thermal conductivity $\lambda = 0.1$ W·m^{-1}·K^{-1} and the thermal diffusivity $D_{th} = 6.4 \times 10^{-8}$ m^2·s^{-1} at 400 K (28), we obtain $\sigma = 0.32$ nm and $\tau = 1.6$ ps. The power of 1 in LJ units corresponds then to $k_BT_c/\tau = 5$ nW, whereas a boundary conductance $G^* = 1$ is equivalent to a real $G = k_B/\tau\sigma^2 = 88$ MW/K/m^2.

To illustrate the relevance of the mapping discussed, we have compared in Fig. 7 the temperature profiles corresponding to the gold/octane interface and to the LJ model, in terms of the reduced temperature T/T_c. The distances have been rescaled here by the value of $\sigma = 0.32$ nm discussed before. For the sake of the comparison, the gold/octane systems have been thermostated at a higher temperature $T = 380$ K than before, because at the reduced temperature $T = 300/569$, the LJ fluid may crystallize. The agreement between the atomically realistic model and the monoatomic LJ model is fairly good. For the lower heating strengths considered, the LJ fluid develops almost the same temperature profile away from the nanoparticle. In particular, the slopes of the temperature profile (flux) at the solid interfaces are quite comparable. Note however, that the temperature jump ΔT at the interface is larger in the case of the LJ model, a fact that can be attributed to the slightly smaller values of the interfacial conductances of the monoatomic model compared with the more realistic system. For higher heating powers, the LJ temperature lies slightly above the octane curve. However, the fluxes at the solid interfaces are again quite comparable, and the interfacial temperature jumps ΔT compare well, probably because of the rapid decrease of the gold/octane conductance with the supplied power.

We have carried out a similar analysis for the gold/water system. The values retained are $\lambda = 0.58$ W/m/K and $D_{th} = 1.3 \times 10^{-7}$ m^2/s for the conductivity and thermal diffusivity at $T = 450$ K, and $T_c = 650$ K for the critical temperature. This yields $\sigma = 0.22$ nm, $\tau = 0.384$ ps, and $\varepsilon/k_B = 602$ K. for the unit of length, time, and energy, respectively. The values of the length and time units are smaller than their gold/octane counterparts, because of the larger thermal conductivity of water. As a consequence, the units of power $P = 21.6$ nW and interfacial conductance $G = 537$ MW/m^2/K are larger than in the previous case. Because of the complexity of the interatomic potentials involved in the water/gold system, we have used a different approach than in the gold/octane case to adjust the solid–liquid interaction parameter for the "corresponding" LJ system. The reduced temperatures T/T_c of the nanoparticles where chosen to be identical, and the parameter c was chosen such that the power input is similar in both cases. This essentially amounts to matching the interfacial conductances of the 2 systems. The resulting value $c = 0.78$ leads to an interfacial work ratio $r = 1.56$. This is slightly different from the value $r = 1.9$ based on the gold/water interfacial work $\pi\rho_{Au}\rho_O\varepsilon_{O/Au}\sigma_{O/Au}^4/3 \simeq 0.13$ kcal/mol/A^2 and the water surface tension $\gamma \simeq 40$ mJ/m^2 at 450 K (17). This difference is probably due to the more complex structure of the gold–water interface, which implies that a simple matching based on identifying the r parameters is not appropriate.

When the matching is performed on the interfacial conductance, the agreement between the 2 temperature profiles, shown in Fig. 8, is very good. That this is the case may seem obvious, because the main macroscopic parameters have been matched. However, the fact that the agreement is obtained down to subnanometer scales, in a situation where heat fluxes are extremely strong and can be transferred to different values of the power input, is far from trivial.

In conclusion, the simple monoatomic LJ model, with an appropriate choice of the parameters, can be used to reproduce quantitatively the features of heat transfer around a nanoparticle obtained for systems with more complex interactions. It constitutes a simple and efficient tool to explore heat transfer at the nanoscale, in the spirit of a coarse-graining approach of such mesoscale phenomena.

Conclusions

We have explored the phenomenon of heat transfer in the vicinity of strongly heated nanoparticles, using molecular dynamics simulations of atomically realistic models or of more coarse-grained LJ monoatomic fluids. The comparison between the 2 approaches shows that, provided the mapping is carried out

by using the physically relevant properties, they are quantitatively equivalent. The simulations reveal that the fluid in the vicinity of the nanoparticles can sustain very high heat fluxes and large temperature differences without undergoing the type of drying instability that is observed on flat surfaces and that temperatures much above the critical temperatures can be reached without observing phase coexistence. In the case of gold in octane, high heat fluxes and temperatures can result in a partial disintegration of the nanoparticle, whereas in the gold in water case, they result only in melting of the particle for comparable heating powers.

The phenomena that are involved in such experiments are quite complex, with a combination of phase transition, interfacial phenomena, and transport phenomena, all taking place on the nanometer scale. It is therefore not trivial that a simple coarse graining based on a matching of interface and thermal properties results in a correct description of the phenomenon. This implies that coarse-grained methods should be appropriate for describing similar phenomena in nanostructures of larger dimensions (e.g., aggregates of nanoparticles or nanostructured surfaces). The level of coarse graining and the gain in efficiency provided by the monoatomic LJ fluid could be even improved by extending to appropriately adapted versions of other coarse graining approaches such as free-energy models (29) or appropriate versions of dissipative particle dynamics (30).

ACKNOWLEDGMENTS. We acknowledge many fruitful interactions with L .J. Lewis. Part of the simulations were realized by using the LAMMPS package (31). This work was supported by French National Agency for Research Project Opthermal.

1. Eastman JA, Phillpot SR, Choi SUS, Keblinski P (2004) Thermal transport in nanofluids. *Annu Rev Mater Res* 34:219.
2. Keblinski P, Prasher R, Eapen J (2008) Thermal conductance of nanofluids: is the controversy over? *J Nanoparticle Res* 10:1089–1097.
3. Prasher R., et al. (2006) Effect of aggregation on thermal conduction in colloidal nanofluids. *Appl Phys Lett* 89:143119.
4. Vladkov M, Barrat J-L (2008) Modeling thermal conductivity and collective effects in a simple nanofluid. *J Comput Theor Nanosci* 5:187.
5. Radunz R, Rings D, Kroy K, Cichos F (2009) Hot Brownian particles and photothermal correlation spectroscopy. *J Phys Chem A* 115:1674.
6. Hirsch LR, et al. (2003) Nanoshell-mediated near-infrared thermal therapy of tumors under magnetic resonance guidance. *Proc Natl Acad Sci USA* 100:13549–13554.
7. Hamaguchi S, et al. (2003) Selective hyperthermia using magnetoliposomes to target cervical lymph node metatstasis in a rabbit tongue tumor model. *Cancer Sci* 94:834–839.
8. Hu M, Petrova H, Hartland GV (2004) Investigation of the properties of gold nanoparticles in aqueous solution at extremely high lattice temperatures. *Chem Phys Lett* 391:220–224.
9. Plech A, Kotaidis V, Grésillon S, Dahmen C, von Plessen G (2004) Laser-induced heating and melting of gold nanoparticles studied by time-resolved X-ray scattering *Phys Rev B* 70:195423.
10. Kotaidis V, Dahmen C, von Plessen G, Plech A, Kong QY (2006) Excitation of nanoscale vapor bubbles at the surface of gold nanoparticles in water. *J Chem Phys* 124:184702.
11. Wang XQ, Mujumdar AS (2007) Heat transfer characteristics of nanofluids: A review. *Int J Thermal Sci* 46:1.
12. Dou, YS; Zhigilei, LV; Winograd N, Garrison BJ (2001) Explosive boiling of water films adjacent to heated surfaces: A microscopic description. *J Phys Chem A* 105:2748–2755.
13. Merabia S, Keblinski P, Joly L, Lewis LJ, Barrat JL (2009) Critical heat flux around strongly heated nanoparticles. *Phys Rev E* 79:021404.
14. Cornell WD, et al. (1995) A second generation force field for the simulation of proteins, nucleic acids, and organic molecules. *J Am Chem Soc* 117:5179–5197.
15. Xia TK, Ouyang J, Ribarsky MW, Landman U (1992) Interfacial alkane films. *Phys Rev Lett* 69:1967–1970.
16. Wilson OM, Hu X, Cahill DG, Braun PV (2002) Colloidal metal particles as probes of nanoscale thermal transport in fluids. *Phys Rev B* 66:224301.
17. Vega C, de Miguel E (2007) Surface tension of the most popular models of water by using the test-area simulation method. *J Chem Phys* 126:154707.
18. Bewig KW, Zisman WA (1965) The wetting of gold and platinum by water. *J Phys Chem* 69:4238–4242.
19. Schrader ME (1970) Ultrahigh-vacuum techniques in the measurement of contact angles. II. Water on gold. *J Phys Chem* 74:2313–2317.
20. Schravendijk P, van der Vegt N, Delle Site N, Kremer K (2005) Dual-scale modeling of benzene adsorption onto Ni(111) and Au(111) surfaces in explicit water. *Chem Phys Chem* 6:1866–1871.
21. Rowlinson JS, Widom R (1982) *Molecular Theory of Capillarity* (Oxford Univ Press, Oxford).
22. Shenogina N, Godawat R, Keblinski P, Garde S (2009) How wetting and adhesion affect thermal conductance of a range of hydrophobic to hydrophilic aqueous interfaces. *Phys Rev Lett* 102:156101.
23. Vladkov M., Barrat J-L (2006) Modelling transient absorption and thermal conductivity in a simple nanofluid. *Nano Lett* 6:1224.
24. Xue L, Keblinski P, Phillpot SR, Choi SUS, Eastman JA (2003) Two regimes of thermal resistance at a liquid–solid interface. *J Chem Phys* 118:337–339.
25. Barrat J-L, Chiaruttini F (2003) Kapitsa resistance at the liquid solid interface. *Mol Phys* 101:1605–1615.
26. Ge Z, Cahill DG, Braun PV (2006) Thermal conductance of hydrophilic and hydrophobic interfaces. *Phys Rev Lett* 96:186101.
27. Palmer BJ (1994) Calculation of thermal-diffusion coefficients from plane-wave fluctuations in the heat energy density. *Phys Rev E* 49:2049–2057.
28. Watanabe H, Seong DJ (2002) The thermal conductivity and thermal diffusivity of liquid n-alkanes. *Int J Thermophys* 23:337–356.
29. Biben T, Joly L (2008) Wetting on nanorough surfaces. *Phys Rev Lett* 100:186103.
30. Avalos JB, Mackie AD (1997) Dissipative particle dynamics with energy conservation. *Europhys Lett* 40:141–146.
31. Plimpton S (1995) Fast parallel algorithms for short-range molecular-dynamics. *J Comput Phys* 117:1–19.